

AD-781 957

FIBER-MATRIX DISPLACEMENT DURING THE
COMPRESSIVE PHASE OF SHOCK LOADING

George E. Hauver

Ballistic Research Laboratories
Aberdeen Proving Ground, Maryland

May 1974

DISTRIBUTED BY:

The logo for the National Technical Information Service (NTIS) features the letters "NTIS" in a large, bold, sans-serif font. A diagonal line strikes through the "N" and "T" from the top-left to the bottom-right.

National Technical Information Service
U. S. DEPARTMENT OF COMMERCE
5285 Port Royal Road, Springfield Va. 22151

Destroy this report when it is no longer needed.
Do not return it to the originator.

Secondary distribution of this report by originating
or sponsoring activity is prohibited.

Additional copies of this report may be obtained
from the National Technical Information Service,
U.S. Department of Commerce, Springfield, Virginia
22151.

ACCESSION FOR	
NTIS	Write Section <input checked="" type="checkbox"/>
D. C.	Dist. Section <input type="checkbox"/>
UNCLASSIFIED	<input type="checkbox"/>
JUSTIFICATION	
BY	
DISTRIBUTION AVAILABILITY CODES	
Dist.	Availability of SPECIAL
A	

The findings in this report are not to be construed as
an official Department of the Army position, unless
so designated by other authorized documents.

*The use of trade names or manufacturers' names in this report
does not constitute indorsement of any commercial product.*

ia

UNCLASSIFIED

SECURITY CLASSIFICATION OF THIS PAGE (When Data Entered)

REPORT DOCUMENTATION PAGE		READ INSTRUCTIONS BEFORE COMPLETING FORM
1. REPORT NUMBER MEMORANDUM REPORT NO. 2383	2. GOVT ACCESSION NO.	3. RECIPIENT'S CATALOG NUMBER AD 781 957
4. TITLE (and Subtitle) Fiber-Matrix Displacement During the Compressive Phase of Shock Loading	5. TYPE OF REPORT & PERIOD COVERED Memorandum Report	
	6. PERFORMING ORG. REPORT NUMBER	
7. AUTHOR(s) George E. Hauver	8. CONTRACT OR GRANT NUMBER(s)	
9. PERFORMING ORGANIZATION NAME AND ADDRESS US Army Ballistics Research Laboratories Terminal Ballistics Laboratory Aberdeen Proving Ground, Maryland	10. PROGRAM ELEMENT, PROJECT, TASK AREA & WORK UNIT NUMBERS Program Element 6.11.02B DA IT061102B33A AMCMS Code 611102.11.85800	
11. CONTROLLING OFFICE NAME AND ADDRESS	12. REPORT DATE MAY 1974	
	13. NUMBER OF PAGES 42	
14. MONITORING AGENCY NAME & ADDRESS (if different from Controlling Office)	15. SECURITY CLASS. (of this report) UNCLASSIFIED	
	15a. DECLASSIFICATION/DOWNGRADING SCHEDULE	
16. DISTRIBUTION STATEMENT (of this Report) Approved for public release; distribution unlimited.		
17. DISTRIBUTION STATEMENT (of the abstract entered in Block 20, if different from Report)		
18. SUPPLEMENTARY NOTES NATIONAL TECHNICAL INFORMATION SERVICE Springfield, VA 22151		
19. KEY WORDS (Continue on reverse side if necessary and identify by block number) Fiber-reinforced composite; Composite debonding; Fiber-matrix displacement; Shock waves; Compressive waves; Electromagnetic gage technique.		
20. ABSTRACT (Continue on reverse side if necessary and identify by block number) Electromagnetic-gage type measurements were performed to determine fiber (wire)-matrix displacement during the compressive phase of shock loading. Fiber diameter and shock impedance were the variables investigated. The relative displacement was found to increase with the fiber diameter, but data for each fiber material could be well represented by a single curve if fiber diameter was used as the unit of relative displacement and shock transit time through the fiber diameter was used as the unit of time. Fibers attained the matrix velocity after a maximum, (normalized relative) displacement which varied linearly as the three-halves power of the shock impedance.		

DD FORM 1473 1 JAN 73 EDITION OF 1 NOV 65 IS OBSOLETE

UNCLASSIFIED

SECURITY CLASSIFICATION OF THIS PAGE (When Data Entered)

TABLE OF CONTENTS

	Page
LIST OF ILLUSTRATIONS	5
LIST OF SYMBOLS	7
I. INTRODUCTION	9
II. EXPERIMENTATION	9
A. General Description	9
B. Electromagnetic-Gage Technique	11
C. Preliminary Experiment	16
D. Investigation of an Epoxy Matrix	18
E. Investigation of a PTFE Matrix	20
F. Tests with a HDPE Matrix	25
III. ANALYSIS	27
IV. RESULTS	33
V. DISCUSSION AND CONCLUSIONS	38
REFERENCES	41
DISTRIBUTION LIST	45

LIST OF ILLUSTRATIONS

Figure	Page
1. Experimental Configuration	12
2. Basic Configuration for Electromagnetic-Gage Type Measurements	14
3. Arrangement of Test Instrumentation	16
4. Oscillogram Showing a Current Pulse and a Trigger-Foil Signal	17
5. Oscillograms from the Preliminary Test	19
6. Preparation of G7 Epoxy Assemblies	21
7. Oscillograms from the Experiment with an Epoxy Matrix	23
8. Oscillograms from the First Experiment with a PTFE Matrix	25
9. Oscillograms from the Second Experiment with a PTFE Matrix	26
10. Configuration of the HDPE Assemblies	28
11. Oscillograms from the Tests with Tungsten Wire in a HDPE Matrix	30
12. Oscillograms from the Tests with Copper Wire in a HDPE Matrix	31
13. Oscillograms showing Signals from Aluminum Films, 127-Micron Aluminum Wire, and 51-Micron Platinum Wire	32
14. Electrode-Sensing Element Configurations used in the Experiments	34
15. Velocity-Time Curves for Wires in a HDPE Matrix	36
16. Velocity-Time Curves for Wires in a HDPE Matrix	37
17. Normalized Curves showing Displacement of Embedded Wires from the HDPE Matrix	38

Figure	Page
18. Normalized Curves showing Displacement of Embedded Wires from the HDPE Matrix	39
19. Relationship between the Normalized Maximum Relative Displacement and the Shock Impedance, Z , of the Embedded Wire	41

LIST OF SYMBOLS

d	electrode diameter, mm
ℓ	mean length of sensing element, mm
ℓ_0	distance between electrodes, mm
r	radius of Helmholtz coil, mm
t	time, microsecond
u	velocity of sensing element, mm/microsecond
u_f	velocity of aluminum film, mm/microsecond
u_w	velocity of wire, mm/microsecond
B	magnetic flux density, tesla
I	peak current to Helmholtz coil, ampere
L_1	trigger location in the matrix
L_2	velocity-sensor location in the matrix
N	number of coil turns
R_0	initial value of R_m , ohm
R_1	$R_2 - R_m$, ohm
R_2	characteristic impedance of transmission line, ohm
R_c	resistance of transmission line, ohm
R_m	resistance of embedded conductor
V	induced voltage, volt
V_s	signal voltage, volt
X_R	relative displacement, mm
Z_e	shock impedance of electrodes, gram/mm^2 microsecond
Z_i	shock impedance of insulator, gram/mm^2 microsecond

I. INTRODUCTION

Electromagnetic-gage type measurements have been performed to investigate the motion of individual fibers (wires) in a plastic matrix during the compressive phase of shock loading. In the basic electromagnetic gage technique, a metallic conductor is embedded in an insulating material which is placed in a uniform magnetic field. Motion of the embedded conductor produces an emf which may be related to the velocity. The basic technique has been attributed to Zayoisii¹ and was first reported in 1960 by Zaitzev, Rokhil, and Shvedov.² Since then, a number of investigators³⁻¹⁵ have used the technique to measure particle velocity as a function of time in shock and detonation waves. Ramifications of the basic technique have been reported by several investigators.¹⁶⁻¹⁹

In 1969, Johnson⁸ used the basic electromagnetic-gage technique to measure particle velocity-time profiles in explosively loaded polymethylmethacrylate. One of his experiments compared the profiles measured separately by embedded wire and foil. The profile measured by embedded wire was characterized by a longer risetime, and this was interpreted to show that the wire lagged behind the plastic as the shock wave passed. The physical arrangement of Johnson's experiment represents the most elementary form of a fiber-reinforced composite, and the long risetime which he detected relates to one mode of failure which can presumably occur during the compressive phase of shock loading.

A series of experiments was performed to investigate further the motion of wires in a plastic matrix during shock loading. The matrix velocity was measured by an embedded thin metal film and permitted relative displacement of the wire and matrix to be calculated as a function of time. It was assumed that relative displacement as a function of time should depend upon such factors as the mismatch of characteristic impedances, the geometry of the metallic conductor, and the stress amplitude. This report describes the series of experiments which was performed. It discusses the measurement technique, the preparation of test specimens, problems which were encountered, the measurement and analysis of experimental records, test results, and conclusions.

II. EXPERIMENTATION

A. General Description

The experimental configuration used for most of the experiments is shown in Figure 1. A plane shock wave is produced by a 100-mm diameter plane wave lens and a 25-mm thick booster charge of TNT. The plane shock wave is transmitted through a buffer of high-density polyethylene (HDPE) and into the plastic matrix. The plastic matrix is located in a uniform magnetic field which is not indicated in

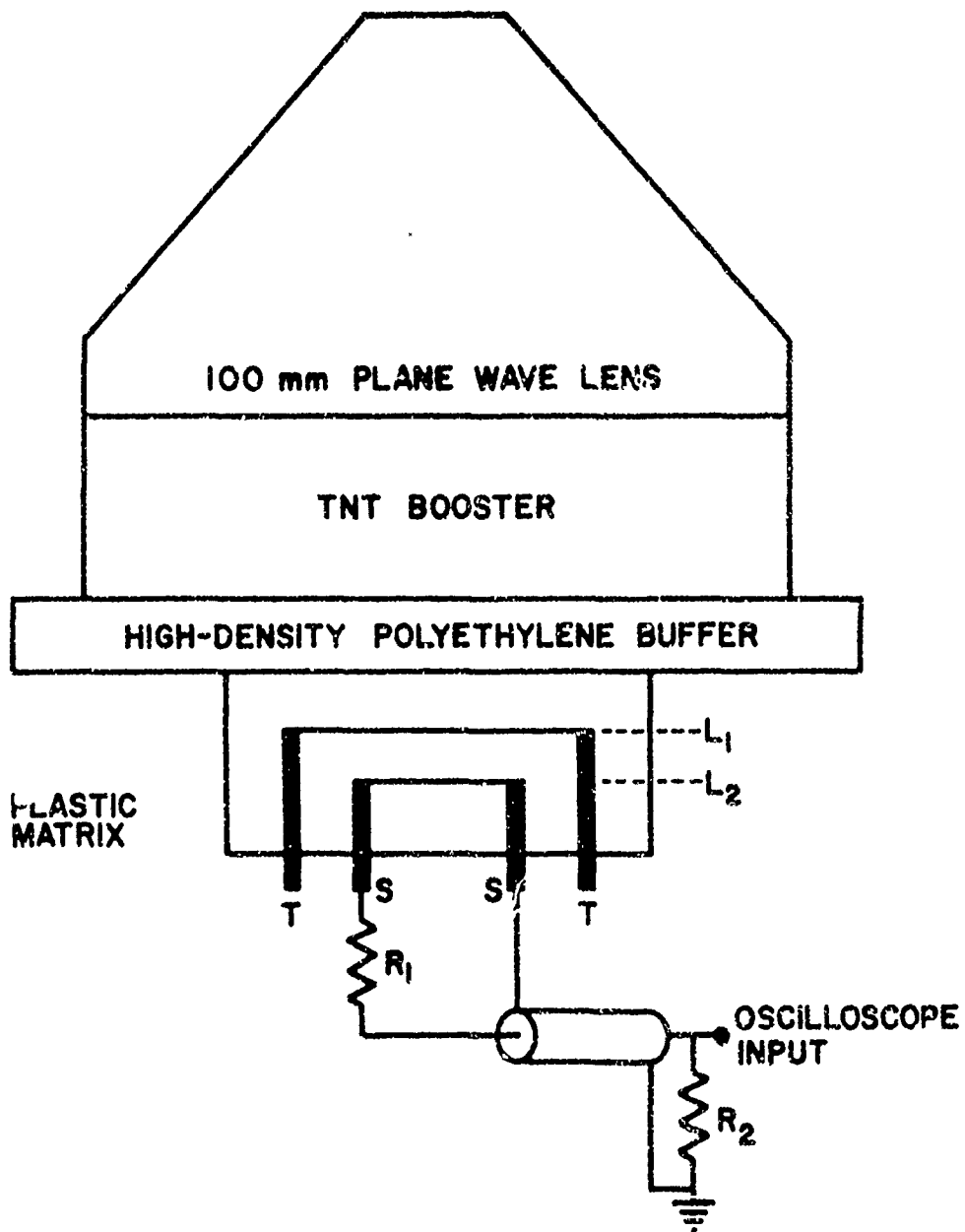


Figure 1. Experimental Configuration

Figure 1, but which is directed perpendicular to the plane of the figure (actually directed up out of the figure). The plastic matrix contains a single metallic film embedded at level L_1 . When this film is set in motion by the shock wave, a voltage signal appears across electrodes TT and is used to trigger the oscilloscopes which observe the signals produced by three conductors at level L_2 . These are in line and only one is indicated in Figure 1. The conductors at L_2 consist of a vapor deposited aluminum film which provides the matrix velocity and two different wires. The conductor embedded at L_1 is located to one side so the shock front arriving at the L_2 conductors is not perturbed. The signal cable shown in Figure 1 is a 5.5-metre length of RG62/U which is terminated at each end by its characteristic impedance.

B. Electromagnetic-Gage Technique

The electromagnetic-gage technique is based on Faraday's law of electromagnetic induction. As shown in Figure 2, a metallic conductor in the shape of a block letter U is embedded in the insulating material to be studied. The sensing element of this conductor has a mean length, ℓ , and is oriented perpendicular to the vector of the particle velocity, u , in the shock wave. The conductor is placed in a uniform magnetic field, B , which is perpendicular to the plane formed by the sensing element and the velocity vector. When the sensing element is set in motion by the incident shock wave, a voltage, V , is induced and appears across SS. In this configuration, the induced voltage is given by the expression,

$$V = B\ell u \text{ (volts)}, \quad (1)$$

where B is in tesla, ℓ is in millimetres, and u is in millimetres/micro-second. An oscilloscope observes the voltage, V_s , where

$$V_s = V \left[\frac{R_2}{R_2 + R_1 + R_m + R_c} \right]. \quad (2)$$

In this expression, R_m is the resistance of the embedded conductor, R_c is the resistance of the coaxial cable, and $R_2 = R_1 + R_m =$ characteristic impedance of the cable.

In the series of tests described by this report, the magnetic field was produced by pulsed Helmholtz coils consisting of six turns of #10 wire with a coil diameter of 610 mm. The coils were powered by the discharge of a 1500 μ F capacitor bank charged to two kilovolts. The maximum current, measured by a noninductive resistor, was usually

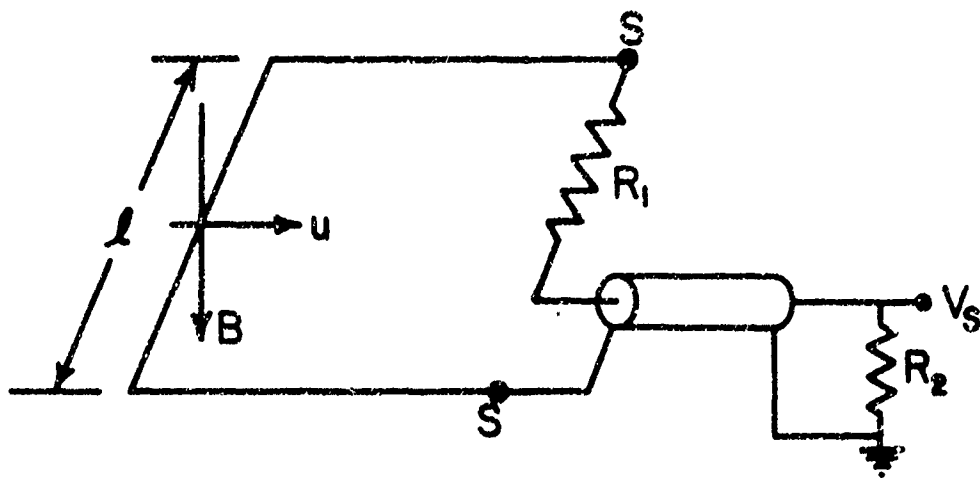


Figure 2. Basic Configuration for Electromagnetic-Gage Type Measurements

in the order of 4.7 kiloamperes, producing a maximum magnetic field of about 83.3 millitesla. Calibration measurements and calculations by Franz²⁰ have shown that the magnetic field calculated from the measured current is in agreement with the measured magnetic field within 0.5 percent, and that the 610-mm diameter coils produce a magnetic field which is uniform within 0.1 percent over a central cube with an edge length of 70 mm.

The arrangement and function of test instrumentation is shown in Figure 3. A test is initiated by a signal from a manually operated trigger source. After a 640 microsecond delay, a detonator unit fires the detonator which initiates the explosive charge shown in Figure 1. The plane shock wave arrives at level L_1 in the matrix approximately 26 microseconds later. The total time of 666 microseconds coincides with the maximum of the current discharge through the Helmholtz coil. After an initial delay of 80 microseconds, the Helmholtz Coil Pulser is triggered. This 80 microseconds delays the current pulse so it is not displayed at the beginning of the oscilloscope sweep. The Helmholtz Coil Pulser is triggered by an exploding wire which injects plasma into a gap in the discharge loop of the capacitor bank. The current pulse is observed differentially across a noninductive resistor R_5 with a resistance of 663 microohms. The lower beam of the 555 oscilloscope is set to be triggerable after a delay of 660 microseconds. This prevents the detonator unit, the Helmholtz Coil pulser, and the inductive signal during field buildup from triggering the lower beam. The lower beam is then triggered internally by the signal S_1 induced when the shock front arrives at level L_1 (See Figure 1). The B-gate output signal then triggers the oscilloscopes which observe signals S_2 , S_3 , and S_4 induced when the shock-front arrives at level L_2 .

A typical record from the 555 oscilloscope is shown in Figure 4. The current trace brightens at the peak when the test is performed. It may be noted that the current pulse is perturbed after the current maximum when the explosive products interact with the coil. In a pretest check, the Helmholtz coil is pulsed and the four oscilloscopes are triggered when the current and field should be maximum. The oscilloscope traces have always been straight and level, indicating that the magnetic field is suitably constant and that inductive effects are negligible. A square wave voltage reference is included in Figure 4 as well as a reference trace used to locate a baseline for the current signal. The signal from the conductor embedded at level L_1 appears at the bottom of the record along with a reference trace used to locate the baseline for the lower signal. This lower signal came from an embedded length of 13 micron thick aluminum foil. While this foil provided a satisfactory trigger signal, aluminum foils were found to provide a lower fidelity measurement of particle velocity than vapor deposited aluminum films.

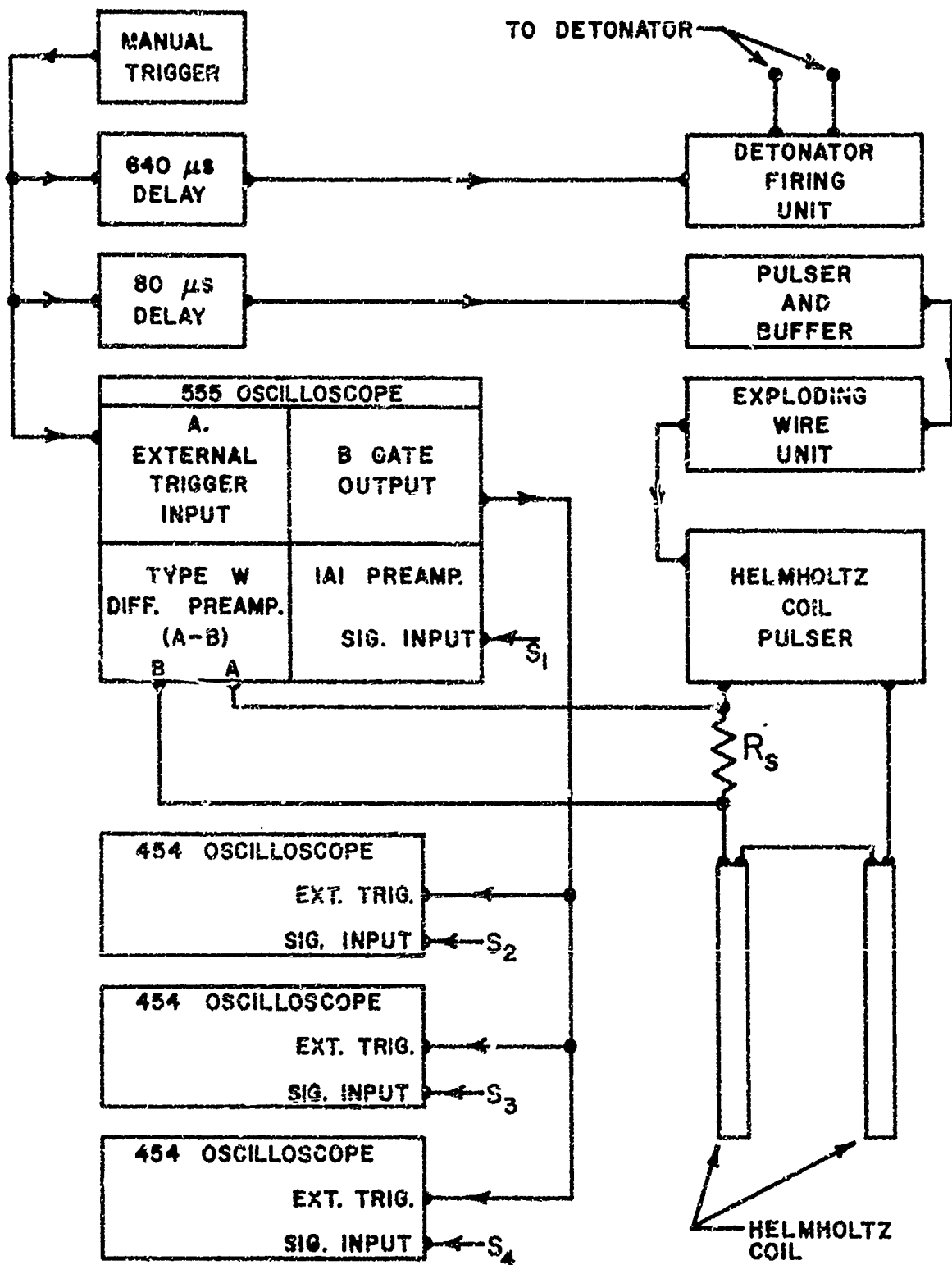
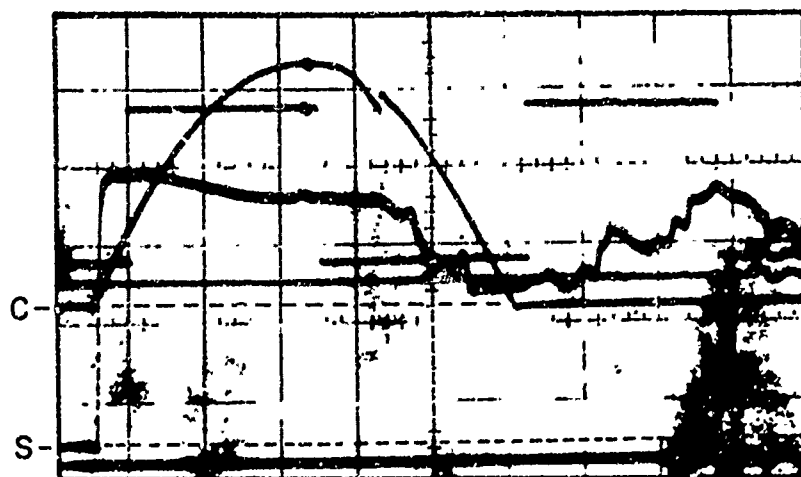


Figure 3. Arrangement of Test Instrumentation



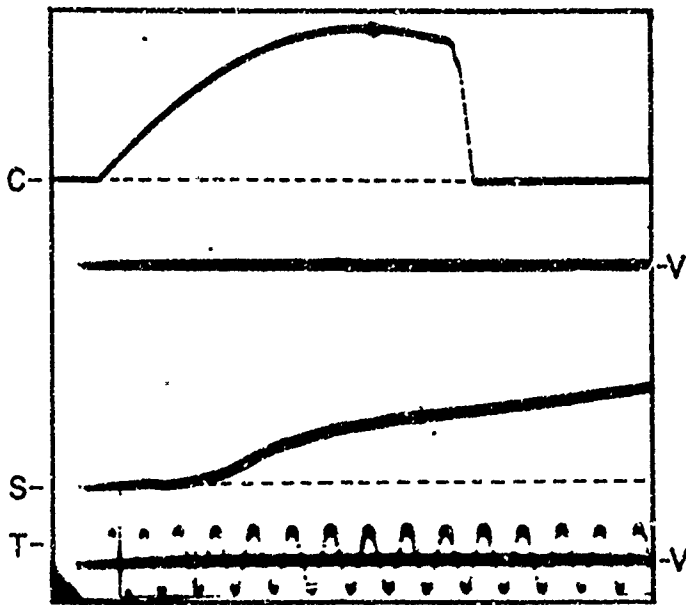
C: CURRENT SIGNAL
S: SIGNAL FROM L₂

Figure 4. Oscilloscope Showing a Current Pulse and a Trigger-Foil Signal

C. Preliminary Experiment

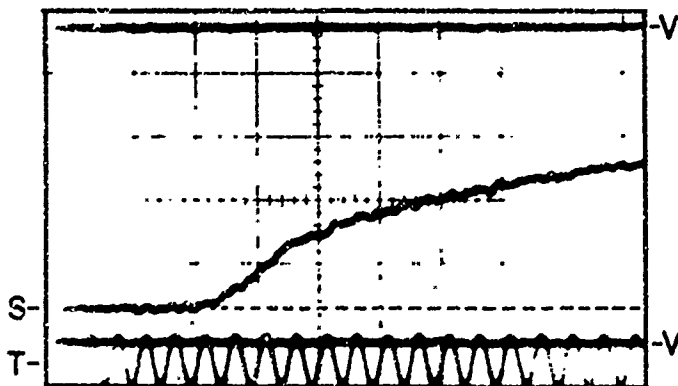
A preliminary experiment was performed to assess the usefulness of the electromagnetic technique for determining fiber-matrix displacement during the compressive phase of shock loading. The experimental arrangement was basically the configuration shown in Figure 1. The matrix material was HDPE, 13 mm thick, with faces flat and parallel within five microns. Copper electrodes, 1.59 mm in diameter, were inserted into the matrix to provide conductor (sensing element) lengths of approximately 12.7 mm. Wires of tungsten and copper, 127 microns in diameter, were placed in contact with the matrix surface and attached to the electrodes by Pb-Sn eutectic solder. (The tungsten wire was plated with a thin coating of copper to facilitate soldering.) A film of aluminum was deposited on the matrix surface by vacuum evaporation, bridging the third pair of copper electrodes. The width of this aluminum film was approximately equal to the electrode diameter. A 6.35-mm thick cover of HDPE was bonded to the surface, covering the sensing elements. The bond was C7A epoxy (Armstrong C7 epoxy with Activator A). The surface of the HDPE cover was ground flat and parallel with the back surface of the matrix within five microns. This assembly was centrally located in the Helmholtz coil and tested, with only minor variations, following the procedure described in Section II-B.

The preliminary test revealed problem areas which were corrected or avoided in subsequent tests. The test oscillograms are shown in Figure 5. The current pulse to the Helmholtz coils is shown in Figure 5-A. A voltage calibration was inadvertently omitted from this record but was recorded on a separate record (not shown) with some loss of reliability. The signal from the tungsten wire is also shown in Figure 5-A. A total sweep time of 200 nanoseconds proved insufficient, for during this time of observation the tungsten wire achieved only about one-half of the matrix velocity. Likewise, the copper wire (See Figure 5-B) achieved only about 65 percent of the matrix velocity in 200 nanoseconds. The signal from the aluminum film is shown in Figure 5-C. A jog occurs at the beginning of this signal. The timing of this jog does not suggest a transmission line problem. If it is assumed that the tungsten and copper wires serve as spacers which cause a bond thickness of about 130 microns and a consequent shock wave transit time of approximately 20 nanoseconds, then the duration of the jog does not correspond to the transit time of the shock wave through the epoxy bond and therefore does not suggest a shock-induced electrical origin. Wave reverberation resulting from an impedance mismatch was also considered. However, the character of the jog does not seem consistent with the anticipated particle velocity in HDPE following an epoxy-aluminum inclusion. Consequently, the origin of the jog has not been satisfactorily resolved. However, it was deemed advisable to reduce the bond thickness in subsequent experiments. It may be noted that the signal from the aluminum film



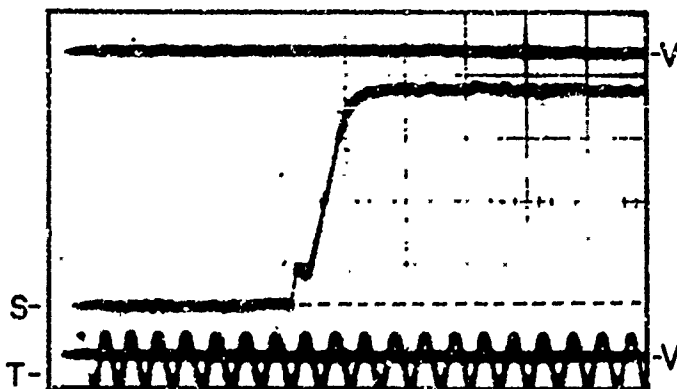
A.

(556 OSCILLOSCOPE)
 C: CURRENT SIGNAL
 S: TUNGSTEN WIRE
 T: 100 MHz
 VV= 1.00 VOLT



B.

(454 OSCILLOSCOPE)
 S: COPPER WIRE
 T: 100 MHz
 VV= 1.00 VOLT



C.

(454 OSCILLOSCOPE)
 S: ALUMINUM FILM
 T: 100 MHz
 VV= 1.00 VOLT

Figure 5. Oscillograms from the Preliminary Test

has a total risetime of from 20 to 25 nanoseconds which is reasonably consistent with shock wave planarity over a distance of 13 mm.

The signals from this test were fully analyzed, but the total time of observation was too short for the results to be related to the results of later analyses which utilized the total time required for wires to attain the matrix velocity. For this reason the analysis for this preliminary test has marginal significance and the results have been omitted.

D. Investigation of an Epoxy Matrix

A series of test assemblies was prepared using Armstrong C7 epoxy as the matrix material. This material was selected for several reasons. First, epoxy is used as the matrix material in practical systems of fiber-reinforced composites. Second, it was anticipated that the use of epoxy would facilitate the fabrication of test assemblies. Third, shock wave data are available for C7 epoxy prepared with both activators A and R (C7A and C7R), and these data show that the choice of activator makes a negligible difference in the high-pressure Hugoniot. Consequently, C7A and C7R could be used interchangeably in preparing assemblies.

The first epoxy assemblies were constructed entirely of C7R and contained the following conductors or sensing elements: 25- and 127- micron diameter Manganin, copper and tungsten; 25- micron diameter aluminum; 127- micron diameter metallized quartz; and the vapor deposited aluminum film which monitored the matrix velocity in each test assembly. Assemblies were prepared as shown in Figure 6. Brass electrodes with a 12.7-mm axial separation were inserted through a C7R disk with the electrode ends projecting into a well formed by a ring of C7R epoxy. Wires were attached to each pair of electrodes with pure tin solder. C7R epoxy was then cast over the wires. The C7R requires an elevated temperature cure and it was found that electrical continuity through the 25 micron aluminum wire and the 127 micron metallized quartz fiber was lost during the curing process. This indicated distortion which was considered undesirable in any of the test assemblies. Consequently, another series of assemblies was prepared using a slightly modified procedure.

The second series of epoxy assemblies was prepared using both C7R and C7A. Again, 1.32-mm diameter electrodes with an axial separation of 12.7 mm were inserted through a disk of C7R epoxy as shown in Figure 6. However, the electrode ends protruded only about 0.25 mm into the well volume. Wires were attached to the electrode ends with eutectic solder with a composition of 44 In-42Sn-14 Cd which melts at 93 degrees Celsius. Room-temperature curing C7A was overcast to a level just covering the wires. After curing, electrodes for the aluminum film were inserted through the C7R base and C7A overcast. Then, additional C7A was overcast to fill the well volume. After curing, the excess

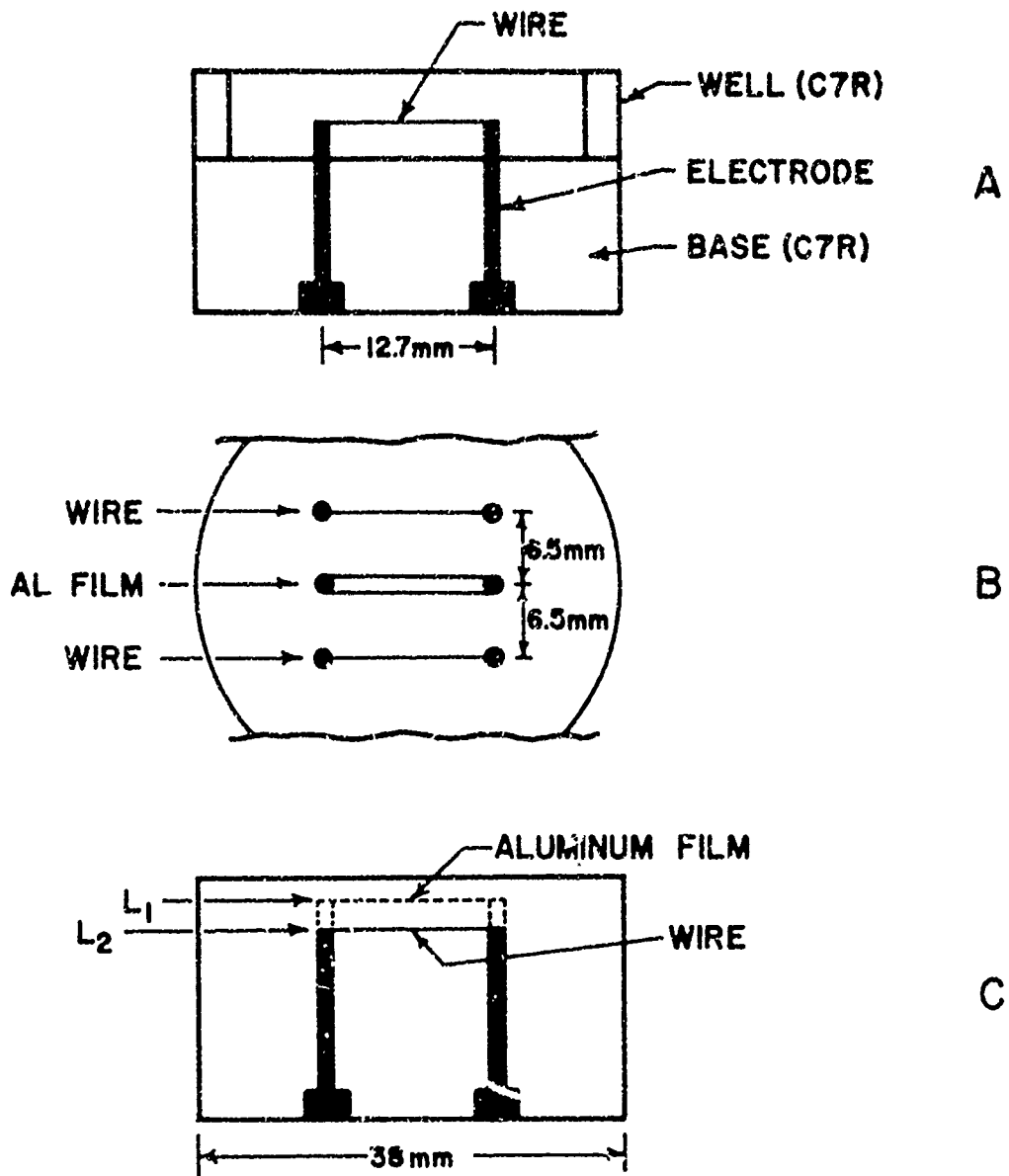


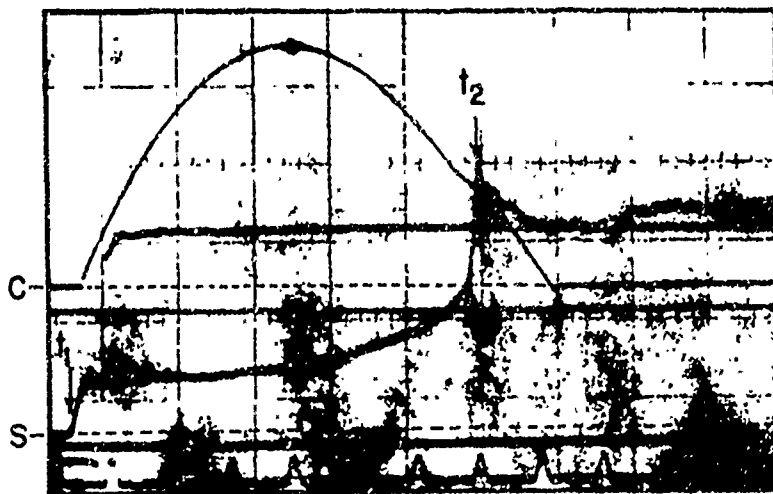
Figure 6. Preparation of C7 Epoxy Assemblies

material was removed to a level L_1 , 1.0 mm above the wire level, L_2 . This machined surface was ground flat and parallel with the base within five microns, leaving the electrode ends exposed at surface level. A 1.32-mm wide strip of aluminum was deposited between the electrode ends by vacuum evaporation. The aluminum films had a resistance of approximately 200 milliohms, indicating a thickness of about three microns. Finally, a 3.2-mm thick cover of C7R epoxy was bonded over level L_1 .

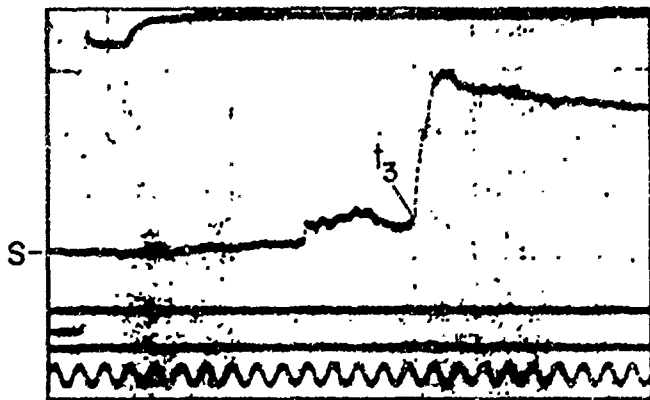
A shock experiment was performed with the assembly containing Manganin wires mounted against a buffer of HDPE as shown in Figure 1. The resistance R_{in} (See Equation 2) was significant in this experiment but the pressure dependence of the resistance is known for Manganin, permitting a correction. The experimental records (oscillograms) from this test are shown in Figure 7. Figure 7-A shows the current pulse (C) and the signal from the aluminum film (S). The signal from the aluminum film actually begins when the shock front enters the epoxy from the HDPE buffer. This reveals that the portion of the signal between times t_1 and t_2 is a shock-induced polarization signal produced by the C7R epoxy cover. It is known that C7 epoxy produces a shock-induced polarization signal, but a signal of this magnitude was not anticipated in this experiment. The polarization signal is accompanied by electrical noise which is superimposed on the following electromagnetic signal. The reason for this electrical noise is not understood but it is frequently observed in conjunction with a polarization signal. The shock-induced signal from the epoxy is also evident in the wire signals shown in Figure 7, B and C. The electromagnetic signals from the wires and film could not be analyzed because of both the electrical noise and distortion produced by the extraneous polarization signal. Consequently, no further tests were conducted using assemblies with a C7 epoxy matrix. Although the reason for a large shock-induced polarization signal was not understood at the time the epoxy series was abandoned, the reason was later found to be an inadvertent deviation from the exact electrical arrangement shown in Figures 1 and 2. This deviation will be explained later. Although there was never time to conduct further tests with the C7-epoxy series of assemblies, it is probable that the exact electrical configuration shown in Figures 1 and 2 would not have produced a troublesome shock-induced polarization signal.

E. Investigation of a PTFE Matrix

The immediate solution to the polarization problem of epoxy was to revert to a nonpolar matrix material. The choice was between HDPE and polytetrafluoroethylene (PTFE), and PTFE was selected primarily for its high temperature stability which was considered an asset in soldering operations. Commercially procured PTFE cylinders were used, and the density near the center where embedded sensing elements



A.
 C: CURRENT SIGNAL
 S: SIGNAL FROM AL
 FILM



B.
 S: SIGNAL FROM 25 μ
 MANGANIN



C.
 S: SIGNAL FROM 127 μ
 MANGANIN

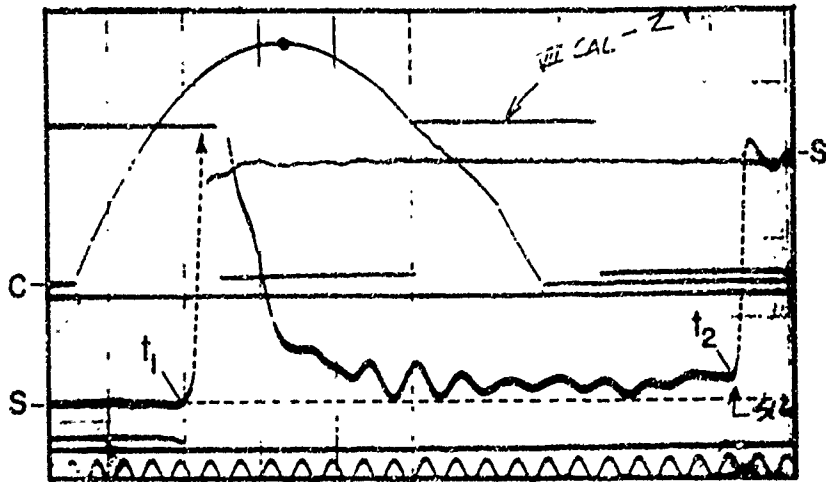
Figure 7. Oscillograms from the Experiment with an Epoxy Matrix

were located was $2.17 \text{ gram/centimetre}^3$ ($2.17 \times 10^3 \text{ kilogram/metre}^3$). The configuration of the wires and aluminum film was the same as that used for the epoxy assemblies (See Figure 6), but the method of assembly was similar to that used previously for the preparation of the HDPE assembly. However, in the PTFE assemblies, the wires were placed in grooves in order to reduce the bond thickness which may have been a problem in the HDPE assembly. Four PTFE assemblies were prepared. These contained 25-, 51-, 79-, and 130- micron diameter tungsten wire; 25-, 76-, and 127- micron diameter copper wire; and 127-micron diameter metallized quartz. Aluminum wire, 25 microns in diameter, could not be used because it broke consistently when the PTFE cover was bonded on. Each of the four assemblies also contained an aluminum film to monitor the matrix velocity.

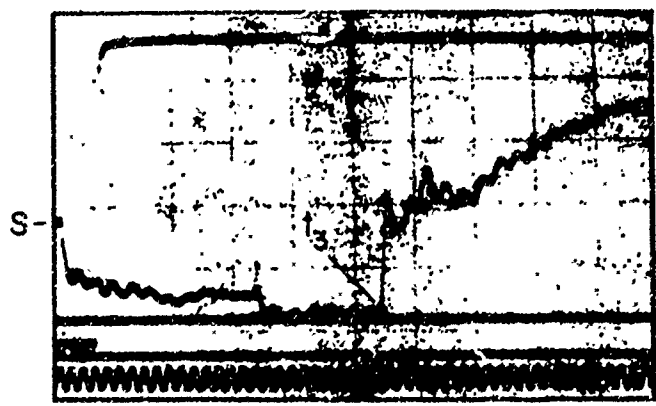
The assembly containing 25- and 127-micron diameter tungsten wire was tested using the configuration shown in Figure 1. The test oscillograms are shown in Figure 8. Figure 8-A shows the current pulse (C) and the signal from the aluminum film (S). As in the case of the test with an epoxy matrix, a shock-induced polarization-type signal begins at time t_1 when the shock front enters the PTFE from the HDPE buffer, and it is not until time t_2 that the shock front arrives at the aluminum film and an electromagnetic signal is observed. This same polarization-type signal also appears on the records of the wire signals (Figure 8, B and C), and it is at time t_3 that the shock front arrives at the plane of the wires. The signals are characterized by electrical noise and distortion similar to the signals from wires in an epoxy matrix (See Figure 7). It seemed unlikely that the polarization-type signal could come from PTFE since shock-induced polarization experiments by the author have indicated that the polarization signal from PTFE is very small. This observation is also confirmed by the electromagnetic gage studies by Franz⁹ in which no shock-induced polarization signal was observed in the course of Hugoniot measurements on PTFE. The polarization signal which troubled this experiment was somewhat reluctantly attributed to a fillet of epoxy which resulted when the PTFE assembly was attached to the HDPE buffer. This reluctance stems from the fact that while a similar fillet of epoxy was used in the test with an epoxy matrix, signal (S) in Figure 7-A shows no evidence of the huge initial spike which appears at time t_1 on signal (S) in Figure 8-A.

A second test with PTFE was conducted using the assembly which contained 25- and 127-micron diameter copper wires. In this test, care was taken to eliminate all polar material from the vicinity of the assembly. The oscillograms from this test are shown in Figure 9. It is evident that the signals from this second test are very similar to the signals from the first test indicating that PTFE is the source of the polarization signal. The polarization signal from the PTFE has a

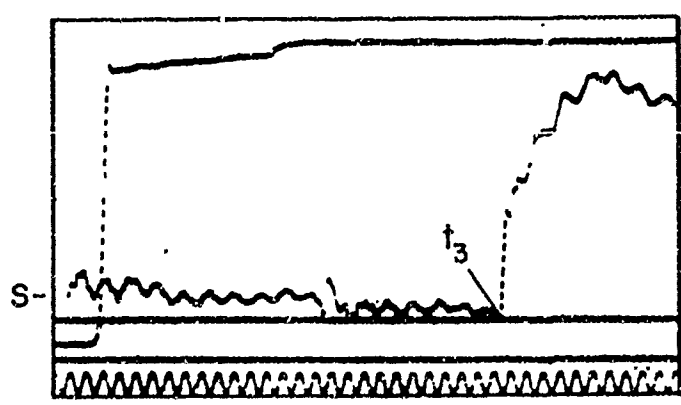
Reproduced from
best available copy.



A.
C: CURRENT
SIGNAL
S: SIGNAL FROM
AL FILM

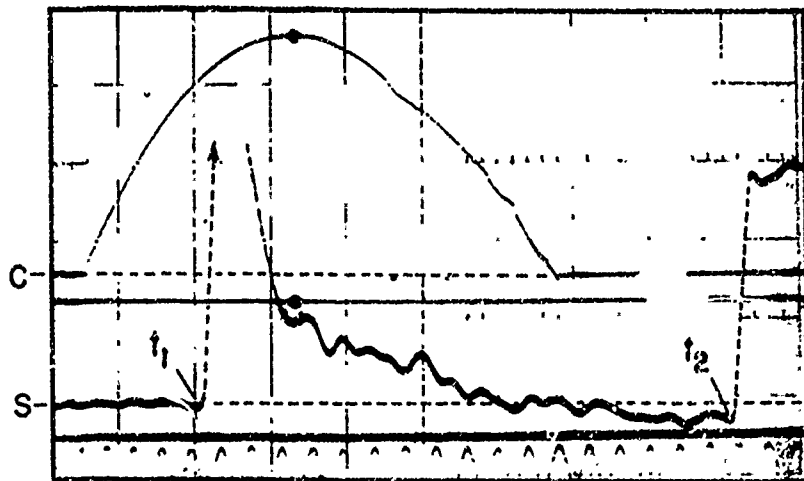


B.
S: SIGNAL FROM 25 μ
TUNGSTEN WIRE

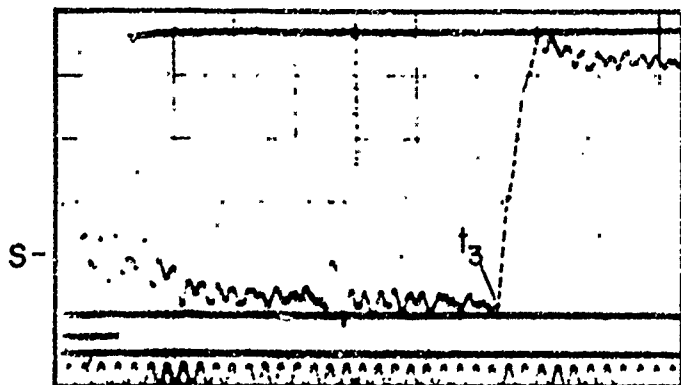


C.
S: SIGNAL FROM 130 μ
TUNGSTEN WIRE

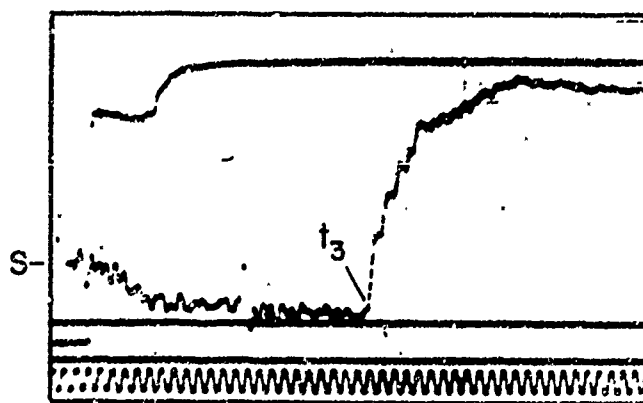
Figure 8. Oscillograms from the First Experiment with
a PTFE Matrix



A.
 C: CURRENT SIGNAL
 S: SIGNAL FROM AL
 FILM



B.
 S: SIGNAL FROM 25μ
 CU WIRE



C.
 S: SIGNAL FROM 127μ
 CU WIRE

Figure 9. Oscillograms from the Second Experiment with a PTFE Matrix

profile which suggests fast relaxation and is similar in appearance to signals from a nonconducting polar liquid.²² In comparison, the polarization signal from C7R epoxy is quite similar to signals from other plastics such as polystyrene or polymethylmethacrylate.²³ In these experiments, it is especially surprising to find that the shock-induced polarization signal from PTFE is larger than the corresponding one from C7R epoxy (if initial amplitudes are compared).

Since the anomalous signal always began after the shock front entered the matrix material from the HDPE buffer, it was evident that no signal came from the HDPE. For this reason it was decided to return to HDPE as the matrix material. A new series of HDPE assemblies was prepared for tests before the cause of the polarization-signal problem was found. The basic cause of the polarization signals is explained by reference to Figure 1. It happened to have been more convenient to place resistor R_1 on the ground side of the embedded conductor.

Consequently, the high resistance path to ground resulted in a relatively large and troublesome polarization signal. Still, the signal from PTFE was inconsistently larger than signals from this material observed in prior shock-induced polarization experiments, and there was some conjecture that the magnetic field may have been influential. However, this point was of secondary interest and could not be pursued. Although the probable source of the anomalous shock-induced signal was found, the new series of HDPE assemblies was completed and HDPE was known from the preliminary experiment to be a trouble-free matrix material. Therefore, tests proceeded with the HDPE series of assemblies.

F. Tests with a HDPE Matrix

The HDPE assemblies were constructed to have the configuration shown in Figure 10. The electrodes were machined from 6-32 brass machine screws, and as shown, were left half threaded. The diameter of the end to which sensing elements were attached was 1.32 mm. These electrodes were forced into undersize holes through the HDPE base. Then the HDPE base was machined and ground to have faces plane and parallel within five microns. The threaded end of each electrode was drilled and tapped to accommodate an 0-80 screw. This provided a mechanical connection and eliminated soldering to attach electrical leads to the completed assembly. As shown in Figure 10, 0.25 mm wide mill saw cuts were made across level L_2 and were just deep enough to accommodate the wires which were connected to the electrodes. Wires were stretched across the saw cuts and soldered to the electrodes with the indium alloy solder which melted at 93 degrees Celsius. A Weller W-TCF2 soldering unit was used and care was taken not to overheat the HDPE matrix. The saw cuts containing the wires were next filled with epoxy. Epon 828 with Activator U was used for the first two assemblies, but it was found to be easier to achieve a bubble-free cast with C7A epoxy and this type was used in the preparation of all subsequent assemblies.

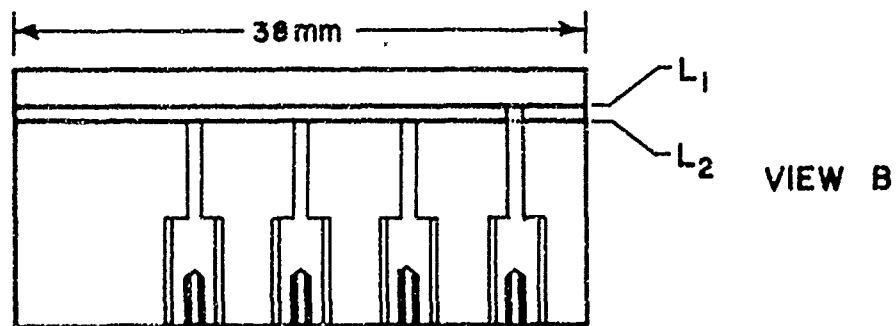
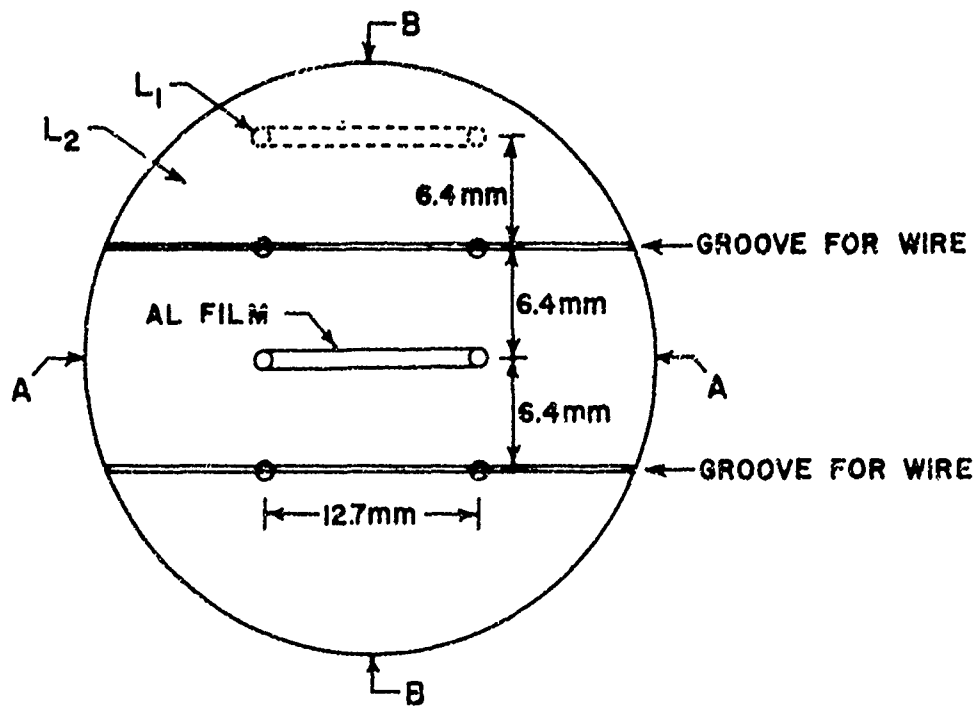
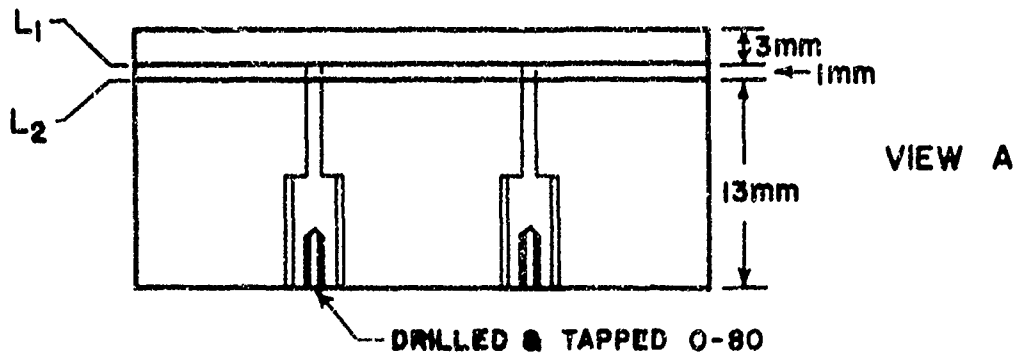


Figure 10. Configuration of the HDPE Assemblies

After a room-temperature cure, the excess epoxy was ground away leaving a plane surface. An aluminum film was next deposited between the center electrodes in level L_2 . The aluminum film had a width of 1.32 mm, a resistance of approximately 200 milliohms, and a consequent thickness of about 300 microns. A cover of HDPE was next bonded over level L_2 using C7A epoxy. A fourth pair of electrodes were then inserted as shown in Figure 10. The assembly was again finished plane and parallel to provide a 1.0 mm spacing between levels L_1 and L_2 .

Aluminum foil, 13 microns thick, was soldered between the electrode ends exposed at level L_1 and a 3.0-mm thick cover of HDPE was bonded over level L_1 . Again the assembly was finished to have faces plane and parallel within five microns. The wires embedded in the HDPE assemblies were 127-micron diameter aluminum; 25-, 51-, and 127-micron diameter copper; 25-, 51-, and 127-micron diameter tungsten; and 51-micron diameter platinum.

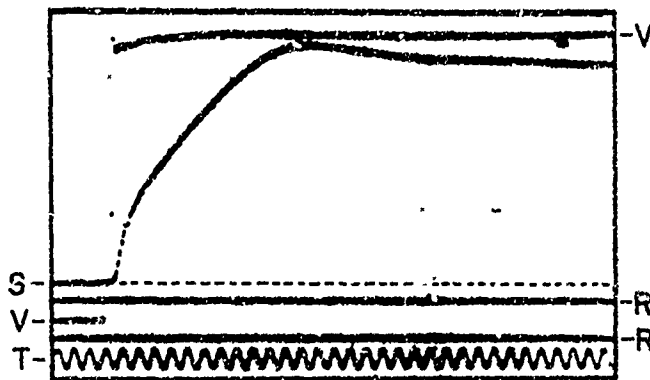
The HDPE assemblies were tested in the experimental configuration shown in Figure 1, using the arrangement of instrumentation shown in Figure 3. Oscillograms from the different tests in the series are shown in Figures 11, 12, and 13. Features of the oscillograms are identified by letter, where T is a timing reference, R is a reference trace, S is the signal from the embedded sensing element, and V is the calibration voltage which was pulsed on to the oscilloscope. The two best signals from aluminum films are shown in Figure 13. The signal risetime of six nanoseconds was the shortest recorded in any of the tests. The 14-nanosecond risetime of the other aluminum film signal was more characteristic of the average shock wave planarity along the length of a sensing element.

III. ANALYSIS

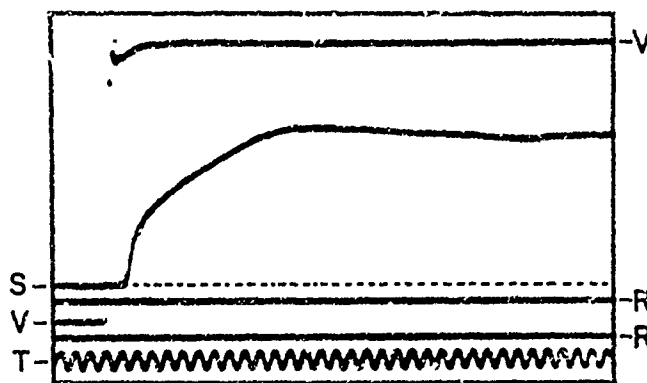
The record of the current pulse was measured to determine the signal amplitude at the time when the matrix was shock loaded. This record (See Figure 4, for example) is actually the voltage drop across resistor R_s (See Figure 3) and the current was determined by dividing the measured amplitude by the resistance of R_s , 663 microohms. The magnetic field was then calculated by the expression,

$$B = 8.992 NI/r, \quad (3)$$

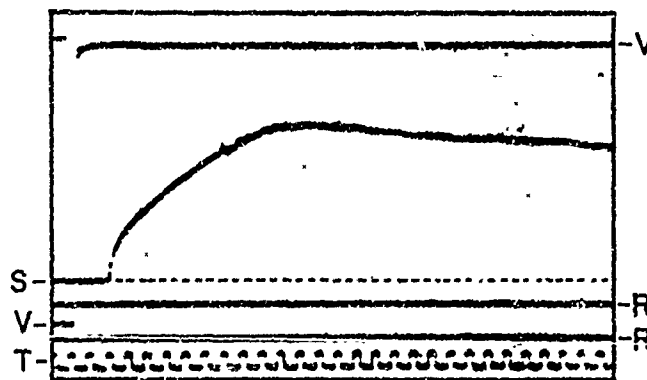
where N is the number of turns of wire on the coil (6), I is the current in amperes, and r is the coil radius in millimetres.



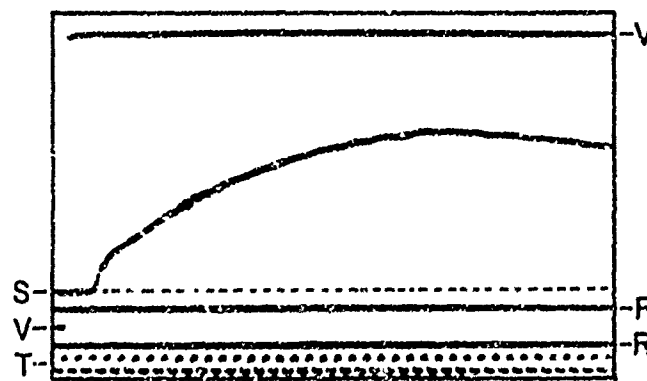
S: 25 μ WIRE
 (TEST 436)
 VV = 1.25 VOLTS
 T = 50 MHz



S: 25 μ WIRE
 (TEST 439)
 VV = 1.75 VOLTS
 T = 50 MHz

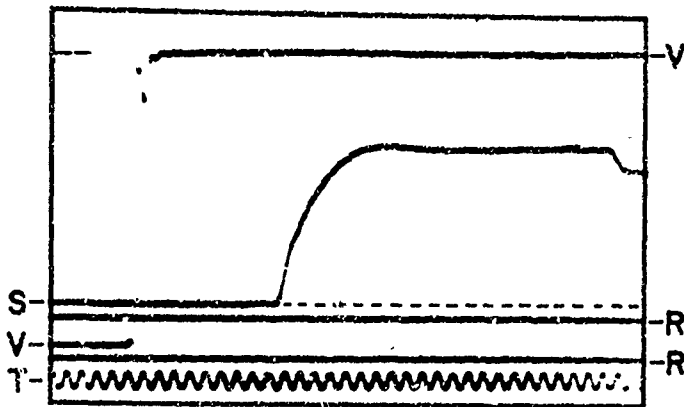


S: 51 μ WIRE
 (TEST 437)
 VV = 1.75 VOLTS
 T = 20 MHz

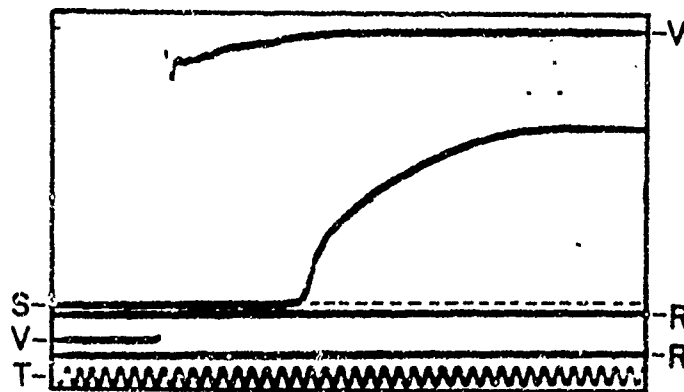


S: 127 μ WIRE
 (TEST 437)
 VV = 1.75 VOLTS
 T = 20 MHz

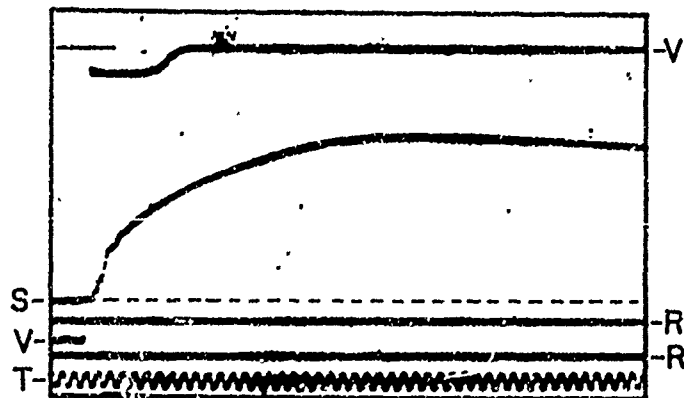
Figure 11. Oscillograms from the Tests with Tungsten Wire in a HDPE Matrix



S: 25 μ WIRE
 (TEST 438)
 VV = 1.75 VOLTS
 T = 100 MHz

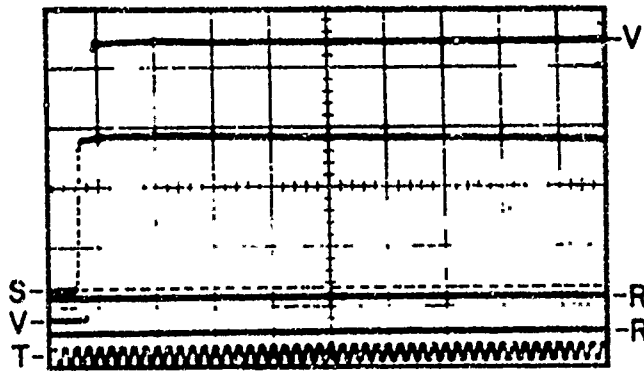


S: 51 μ WIRE
 (TEST 438)
 VV = 1.75 VOLTS
 T = 100 MHz

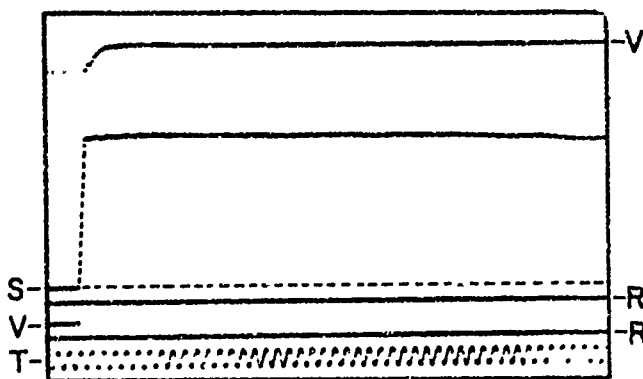


S: 127 μ WIRE
 (TEST 441)
 VV = 1.75 VOLTS
 T = 50 MHz

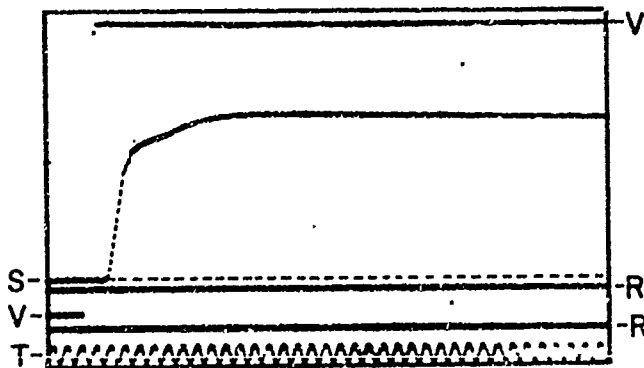
Figure 12. Oscillograms from the Tests with Copper Wire in a HDPE Matrix



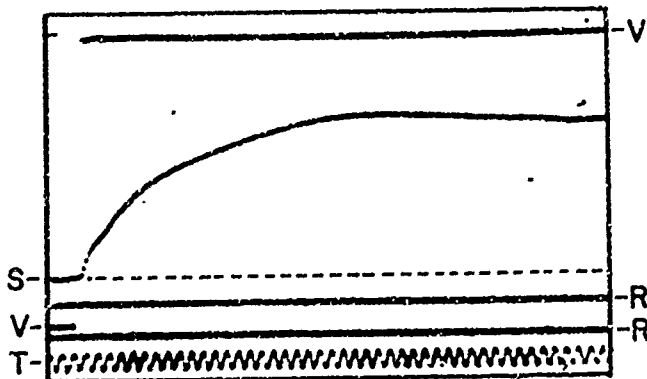
S: AL FILM
 (TEST 441)
 VV=1.75 VOLTS
 T= 50 MHz
 RISETIME = 6 ns



S: AL FILM
 (TEST 440)
 VV=1.75 VOLTS
 T= 50 MHz
 RISETIME = 14 ns



S: 127 μ AL WIRE
 (TEST 440)
 VV=1.75 VOLTS
 T= 50 MHz



S: 51 μ PT WIRE
 (TEST 441)
 VV=1.75 VOLTS
 T= 50 MHz

Figure 13. Oscillograms showing Signals from Aluminum Films, 127-Micron Aluminum Wire, and 51-Micron Platinum Wire

The signals from the aluminum film and the wires were measured to obtain voltage-time curves. These voltage-time curves were converted to velocity-time curves by means of Equation 1. However, there was concern about the length of the sensing element, ℓ , used in

Equation 1. Edwards²³ has shown that, neglecting eddy currents, ℓ is the mean length of the sensing element, and he has indicated that experimental results confirm this. The mean length of the sensing element seems to be well defined in a transverse configuration in which a block-U-shaped foil sensor is introduced from the side and lies entirely in a plane parallel to the incident plane shock front. However, when the electrodes to the sensing element are introduced perpendicular to the plane of the incident shock front, the situation can be more complex. This latter case is depicted in Figure 14 which shows the electrode ends and the sensing element in the plane parallel to the incident shock front. In Figure 14-A, if the impedance of the electrodes (Z_e) is matched to the impedance of the insulating material (Z_i), the mean length of the sensing element should be $(\ell_o + d)$. In the opposite extreme, if ($Z_e \gg Z_i$) the electrodes are rigid while the insulator flows past and the effective length should be approximately ℓ_o . The case of a thin film with a width equal to the electrode diameter is depicted in Figure 14-B. Again, if ($Z_e = Z_i$), the mean length of the sensing element should be $(\ell_o + d)$. In the opposite extreme, if ($Z_e \gg Z_i$) and the electrodes are rigid while the insulator flows past, the mean length of the sensing element should be approximately $[\ell_o + d (1 - \pi/4)]$. In the case of a large mismatch between the impedances of the electrodes and insulator, the behavior of the sensing element in the vicinity of the electrodes is somewhat obscure. In the present case of brass electrodes and a HDPE insulator, ℓ_o has been assumed to be the appropriate mean length for embedded wires with a small diameter. This assumption also leads to the use of $[\ell_o + d (1 - \pi/4)]$ for the mean length of the aluminum film. In the experiments in which a HDPE insulator was used, the electrode diameter (and film width) was 1.32 mm and ℓ_o was approximately 11.4 mm, so the mean length of the film should be $(\ell_o + 0.025 \ell_o)$. Using $1.025 \ell_o$ as the film length, ℓ , the film or matrix velocity was found always to be less than the maximum wire velocity. It is not conceivable that the wire velocity could exceed the matrix velocity. It is conceivable that the wire might appear not to attain the matrix velocity because stretching near the electrodes and shock heating increase the wire resistance until R_m in Equation 2 becomes a significant part of the circuit resistance.

Although resistance-time measurements were not performed during shock loading of any test assemblies, it was not apparent that the film resistance ever increased significantly during a measurement and it is not obvious that wire behavior should be much different. It is reasonable to expect the wire to attain the matrix velocity eventually, and this was the assumption used in reducing test data. It was found that

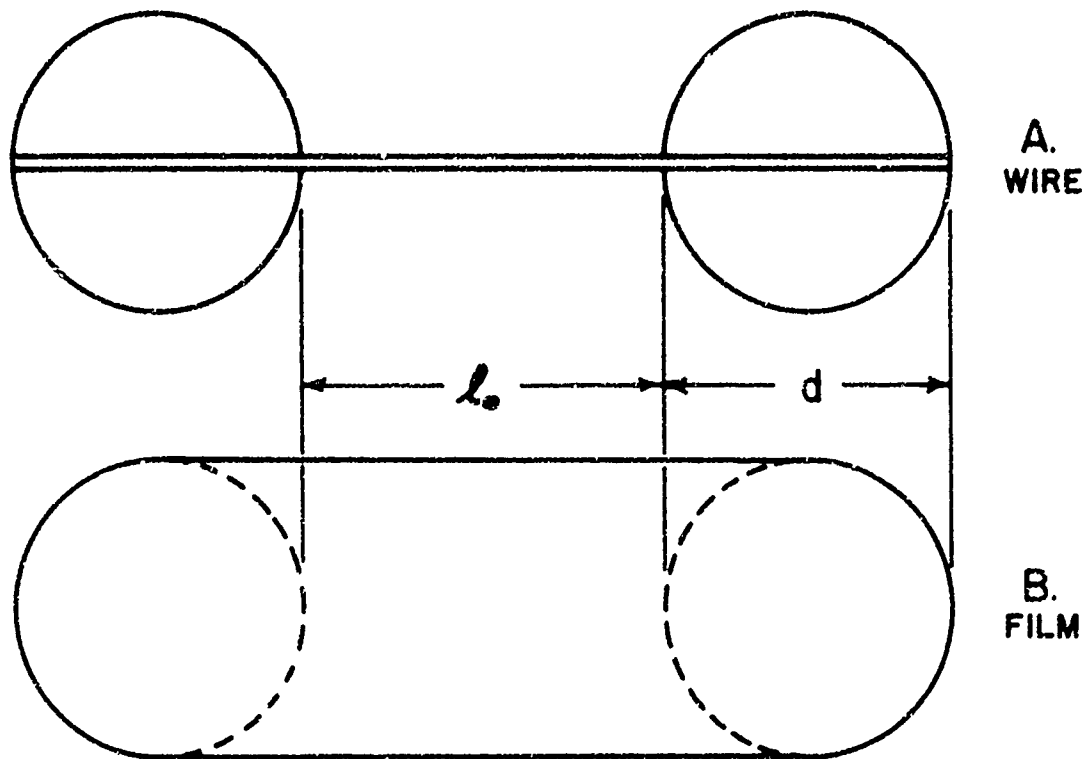


Figure 14. Electrode-Sensing Element Configurations Used in the Experiments

film and wire velocities came into general agreement if the film length was also chosen to be ℓ_0 . Exact agreement between film and wire velocities usually was not achieved. However, the wire velocities were within plus or minus three percent of the film velocity, except in one instance when the wire velocity was plus five percent. Part of the uncertainty in wire velocity is believed to result from variability in the soldered connections at the electrodes. It became evident that three percent agreement was the best that could be expected.

The object of the experiments was to determine the relative displacement of the matrix and the embedded wires. The relative displacement, X_r , is given by the expression,

$$X_r = \int u_f dt - \int u_w dt, \quad (4)$$

where u_f is the film (matrix) velocity, u_w is the wire velocity, and t is time. Small discrepancies between the matrix velocity and the maximum wire velocity introduced unacceptable error in X_r . It was assumed that error in the wire velocity resulted primarily from uncertainty about the effective wire length between the soldered connections. Consequently, small adjustments in wire length were introduced to bring the maximum wire velocity into agreement with the film (matrix) velocity.

Data for the different embedded wires are presented as relative displacement versus time. A useful normalization procedure consisted of using the wire diameter as the unit of relative displacement and the transit time of the initial shock wave along the wire diameter as the unit of time. Finally, normalized relative displacement was examined in terms of shock impedance.

IV. RESULTS

Velocity-time curves for wires embedded in a HDPE matrix are shown in Figures 15 and 16. The matrix velocity is shown in each figure, except at early times where the actual risetime of the signal in each experiment depended upon the shock wave planarity over the film length. The actual risetime of film signals was used in the analyses and adjacent wires were assumed to have been subject to the same nonplanarity. These velocity-time curves were integrated to obtain displacement-time, and relative displacement-time was determined in accordance with Equation 4. The normalized curves of relative displacement versus time are shown in Figures 17 and 18. As the wire approaches the matrix velocity, the relative displacement approaches a maximum, and the dependence of this maximum relative displacement

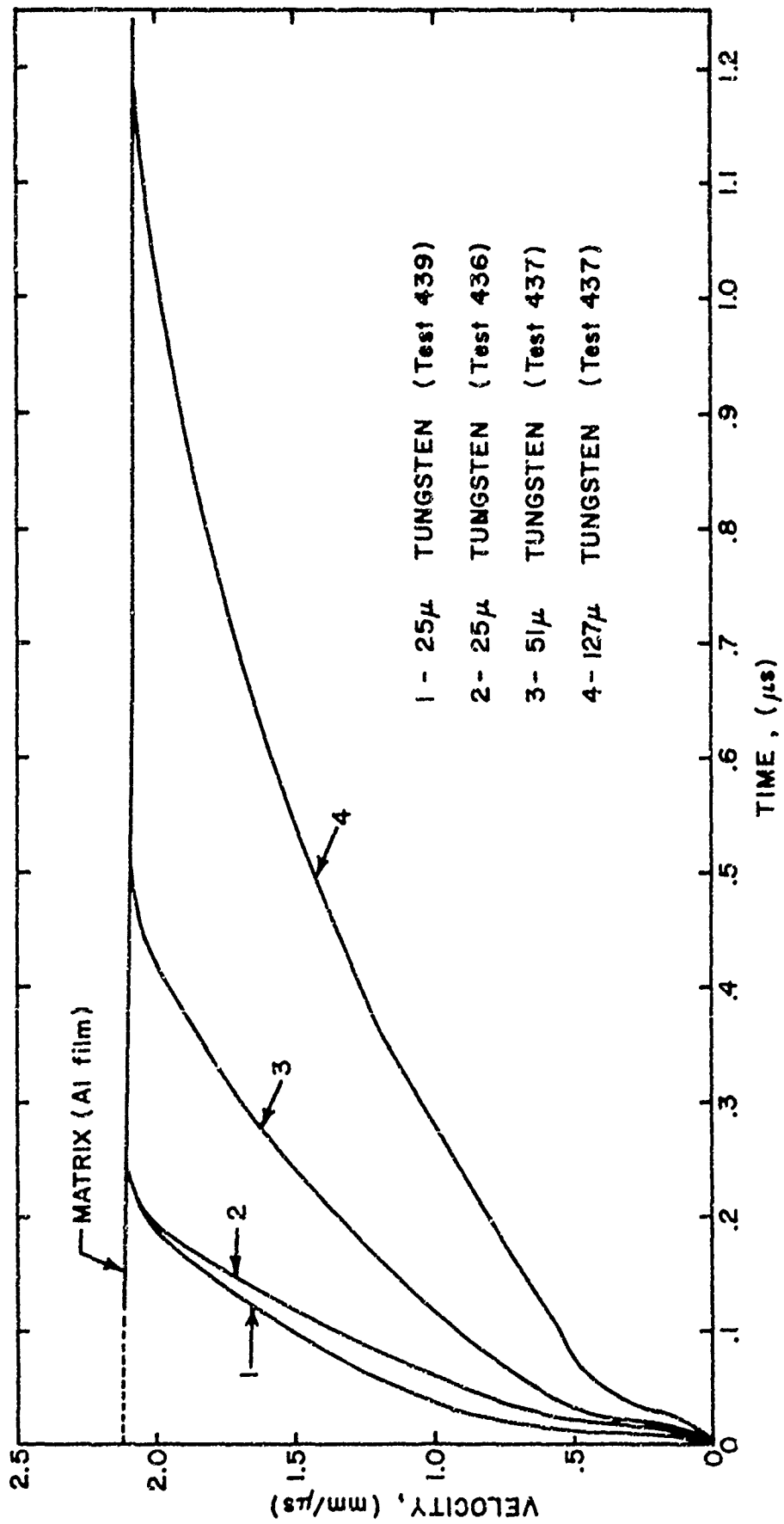


Figure 15. Velocity-Time Curves for Wires in a HDPE Matrix

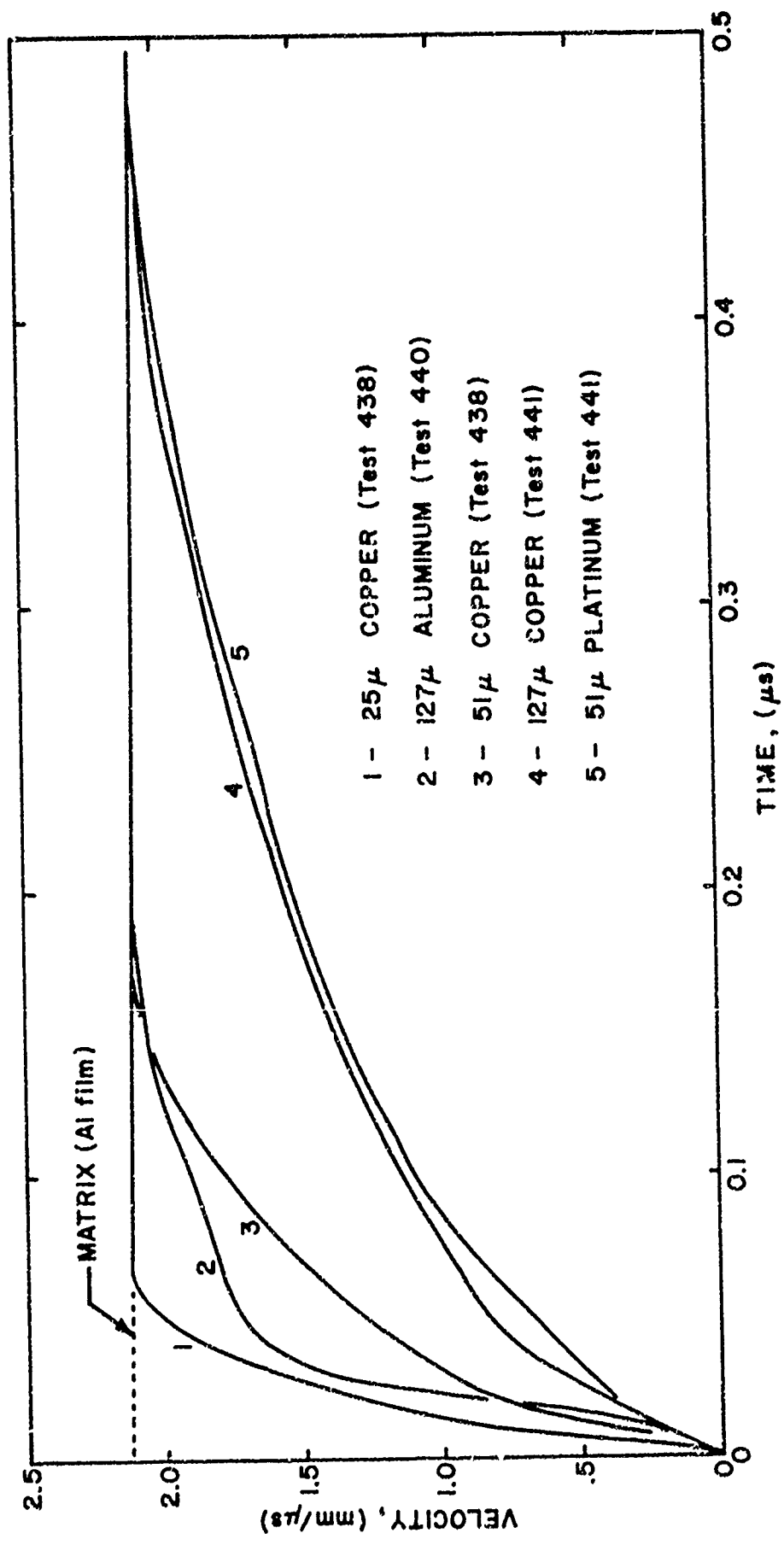


Figure 16. Velocity-Time Curves for Wires in a HDPE Matrix

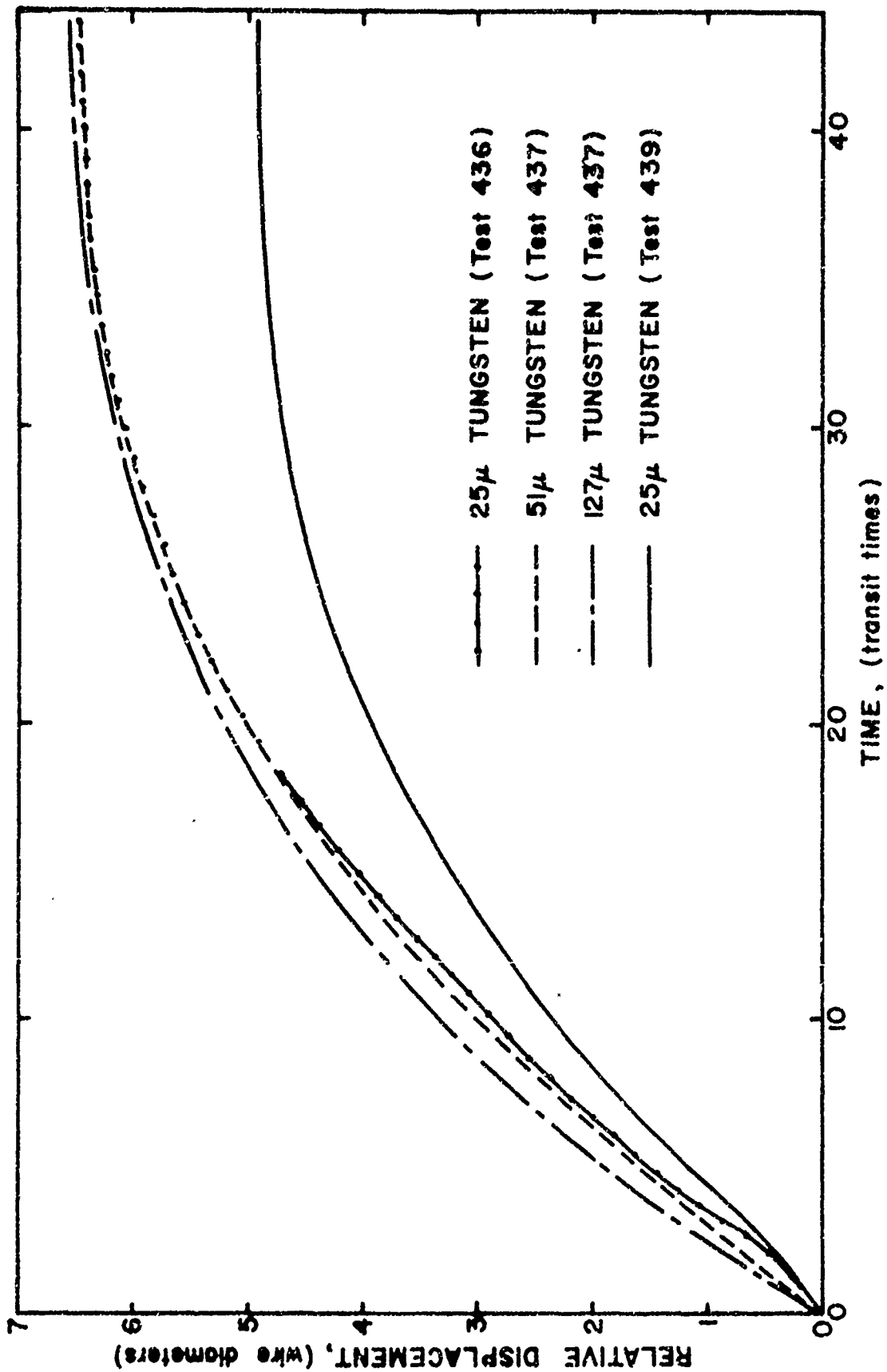


Figure 17. Normalized Curves Showing Displacement of Embedded Wires from the HDPE Matrix

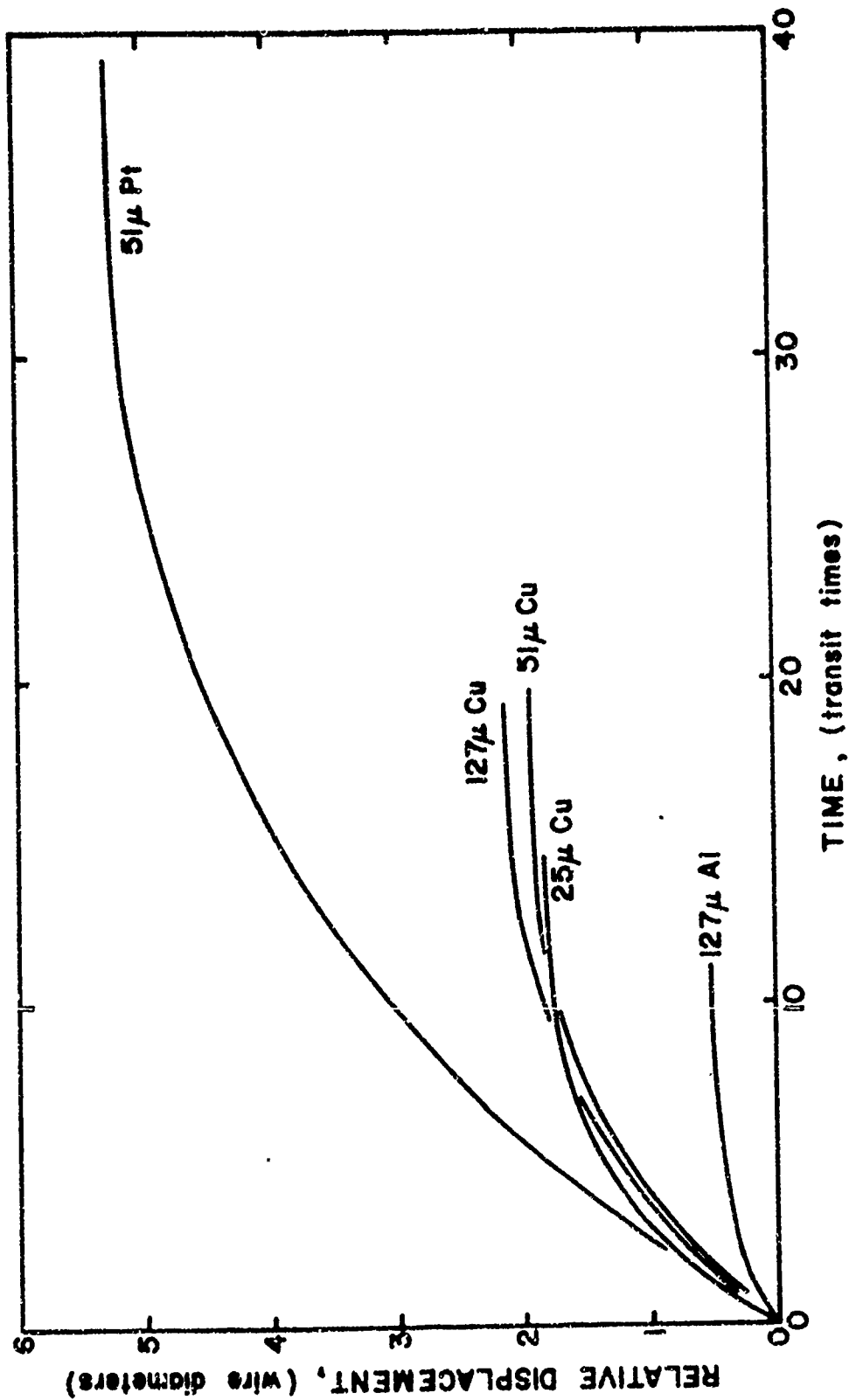


Figure 18. Normalized Curves showing Displacement of Embedded Wires from the HDPE Matrix

on shock impedance (product of initial density and shock velocity) of the wire metal is shown in Figure 19.

V. DISCUSSION AND CONCLUSIONS

The velocity-time curves presented in Figures 15 and 16 generally indicate that the time required for an embedded wire to attain the matrix velocity during the passage of a shock wave increases as the shock impedance of the wire and its diameter. Figures 17 and 18 show that wires of the same metal with different diameters tend to be represented by a single curve if the data are normalized by using wire diameter as the unit of relative displacement and shock transit time through the wire diameter as the unit of time. In Figure 19, the maximum normalized relative displacement is plotted versus the three-halves power of the shock impedance, the three-halves power being used because it yields an essentially linear relationship. The line in Figure 19 is forced through the shock impedance of HDPE since it is assumed that no relative displacement can occur when impedances are matched. A slight deviation from linearity might actually represent the data points for aluminum and copper somewhat better than a straight line. However, a greater concern is the discrepancy in the data for tungsten. It is clearly evident in Figure 19 that the point for 25-micron diameter tungsten from Test 439 is consistent with the data for other metals while the tungsten data for Tests 436 and 437 are displaced far to the right. All of the tests with a HDPE matrix were reviewed, and the only obvious difference was the use of Epon 828-U epoxy to seal the wires into the grooves in Tests 436 and 437, and the use of C7A epoxy in all later tests (See Section on the HDPE matrix). At the shock stress of 127 kilobars (12.7 gigapascals) attained in these experiments, it had been anticipated that shock impedance would be the controlling factor. However, the discrepancy in the tungsten data strongly suggests that even at this high stress level other properties of the matrix are apparently influential. It would have been interesting to investigate this point further, but time and the funding level did not permit such an excursion. In Figure 19, the three points for copper lie in an order which suggests that the normalized maximum relative displacement may increase with the wire diameter. However, the tungsten-wire data from Tests 436 and 437 (See Figure 17) show very close agreement between the normalized curves for 25-, 51-, and 127-micron diameter wires.

The change in resistance of embedded films and wires during shock compression is a concern because if R_m in Equation 2 becomes a significant part of the circuit resistance, the signal amplitude is reduced, and the calculated velocity is erroneously low. The resistance increases for several reasons. First, the embedded conductor is shock compressed and heated. Second, the resistance continues to increase with time after shock compression because the insulator is shock heated to a higher temperature and heat is transferred by conduction

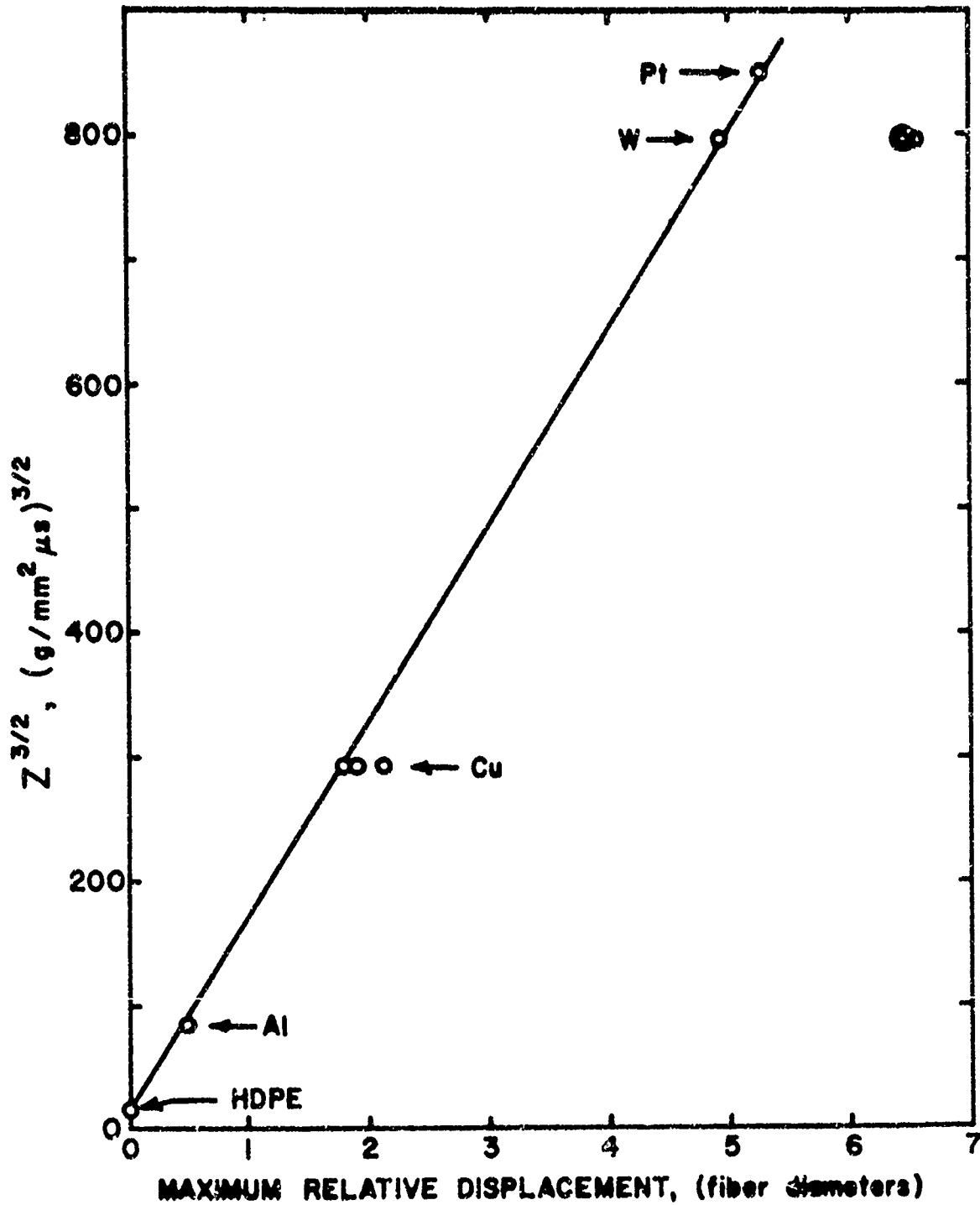


Figure 19. Relationship between the Normalized Maximum Relative Displacement and the Shock Impedance, Z , of the Embedded Wire

to the embedded conductor. Third, the embedded conductor must stretch as the low impedance insulator carries it away from the points where it attached to the high impedance electrodes. Experiments to examine the change in resistance with time were considered but could not be scheduled. However, Franz²⁴ investigated a paraffin-polyethylene system with the same basic configuration of the HDPE experiments. At 127 kilobars (12.7 gigapascals), vapor deposited aluminum films in the paraffin-polyethylene matrix underwent an immediate resistance increase to 1.85 R, where R is the resistance prior to shock compression. Then, after two microseconds of shock compression, the combined effects of stretching and heat transfer had increased the resistance of the aluminum film to only 2.5 R. Since R in the HDPE series of experiments was approximately 200 milliohms, the resistance should not have increased to more than 450 milliohms in the 1.25 microsecond duration of the longest experiment. This increase in resistance could have introduced an error of only 0.25 percent, which is essentially negligible. Franz's unpublished data on shock-induced resistance changes of copper²⁵ showed equivalent increases in the resistance of copper foil and wire under shock compression to a slightly higher stress level.

When the experimental program was planned, it was anticipated that the relative displacement of the wires and matrix should depend on factors including the stress level in addition to wire diameter and shock impedance. It was intended that experiments should be performed at different stress levels. Unfortunately, the problems encountered and the level of support for the effort permitted only one stress level to be investigated. While there would have been greater interest in a lower stress closer to the failure threshold, lower stresses could not be attained when the effort began. These lower stresses are normally attained by low-velocity projectile impact and a suitable gun was not available until late in the study. Consequently, the experiments were performed using explosive loading. Although low stresses can be reached by explosive loading, the practical method employs laminated buffers with impedance-mismatched laminations. Unfortunately, high-impedance laminations are metallic in practical systems and the motion of these metals in the magnetic field causes field compression which could conceivably perturb the measurements. Consequently, a 100-mm diameter plane wave lens with a relatively low energy TNT booster charge was used to load the HDPE buffer directly, and this system produced the test pressure of 127 kilobars (12.7 gigapascals).

Finally, it should be noted that the motions of the embedded wire and the matrix were measured at locations which were well separated in order to prevent interactions. In order to relate the measured relative displacement to actual debonding, it would undoubtedly be necessary to define matrix motion better at locations closer to the wire.

REFERENCES

1. L. V. Al'tshuler, "Use of Shock Waves in High-Pressure Physics," Soviet Physics Uspekhi, Vol. 8, No. 1, 1965, p. 63.
2. L. V. Zaitzev, P. F. Pokhil and K. K. Shvedov, "The Electromagnetic Method for the Measurement of Velocities of Detonation Products," Doklady Acad. Sci. USSR, Vol. 132, No. 6, 1960, pp. 1339-40.
3. J. T. Frasier, "Hypervelocity Impact Studies in Wax," Ballistic Research Laboratories Report No. 1124, February 1961. (AD# 255772)
4. J. T. Frasier and B. G. Karpov, "The Transient Response of Wax Target Subjected to Hypervelocity Impacts," Experimental Mechanics, Vol. 5, 1965, pp. 305-12.
5. V. A. Veretennikov, A. N. Dremin and K. K. Shvedov, "Determination of the Detonation Parameters of Condensed Explosives," Combustion, Explosion and Shock Waves, Vol. 1, No. 3, 1965, pp. 1-5.
6. A. N. Dremin, S. V. Pershin and V. F. Progorelov, "Structure of Shock Waves in KCl and KBr under Dynamic Compression to 200,000 Atmospheres," Combustion, Explosion and Shock Waves, Vol. 1, No. 4, 1965, pp. 1-4.
7. W. J. Gillich and W. O. Ewing, "Measurement of Particle Velocities Associated with Plastic Waves Propagating in Bars," Ballistic Research Laboratories Report No. 1405, June 1968. (AD #837927)
8. E. G. Johnson, "An Electromagnetic Technique for Measuring Particle Velocity in Shock Waves," Rohm and Haas Technical Report S-181, February 1969.
9. R. E. Franz, "An Electromagnetic Measurement of the Shock Hugoniot of Teflon," Ballistic Research Laboratories Memorandum Report No. 2075, 1970. (AD #716333)
10. S. J. Jacobs and D. J. Edwards, "Experimental Study of the Electromagnetic Velocity-Gage Technique," Fifth Symposium on Detonation, Pasadena, California, August 18-21, 1970, Office of Naval Research Report ACR-184, pp. 413-26.
11. D. J. Edwards, J. O. Erkman, and S. J. Jacobs, "The Electromagnetic Velocity Gage and Applications to the Measurement of Particle Velocity in PMMA," Naval Ordnance Laboratory Technical Report No. 70-79, 20 July 1970.
12. D. J. Edwards and E. O. Erkman, "The Measurement of Particle Velocity in Cast TNT," Naval Ordnance Laboratory Technical Report No. 71-19, 14 June 1971.

13. D. J. Edwards, J. O. Erkman and Donna Price, "The Measurement of Particle Velocity in Pressed Tetryl," Naval Ordnance Laboratory Technical Report No. 72-83, 3 August 1972.
14. D. J. Edwards, J. O. Erkman and Donna Price, "The Measurement of Particle Velocity in Pressed TNT," Naval Ordnance Laboratory Technical Report No. 72-82, 18 August 1972.
15. W. S. deRosset, R. E. Franz and P. H. Netherwood, "Fracture with Stress Waves," Army Symposium on Solid Mechanics, Ocean City, Maryland, 27 September 1972.
16. C. Young, R. Fowles, and R. P. Swift, "An Electromagnetic Stress Gage," Physics International Company Technical Report No. 70-10, August 1970 (also presented at the 17th Sagamore Conference on Shock Waves and the Mechanical Properties of Solids, Raquette Lake, New York, 1-4 September 1970).
17. B. Hayes and J. N. Fritz, "Measurement of Mass Motion in Detonation Products by an Axially-Symmetric Electromagnetic Technique," Fifth Symposium on Detonation, Pasadena, California, August 18-21, 1970, Office of Naval Research Report ACR-184, pp. 447-54.
18. J. N. Fritz, R. S. Caird, and R. G. McQueen, "The Use of a Magnetic Field to Measure Particle Velocity I. Basic Concepts and Exploratory Experiments," Los Alamos Scientific Laboratory Report LA-4545-M, December 1970.
19. J. N. Fritz and J. A. Morgan, "An Electromagnetic Technique for Measuring Material Velocity," Los Alamos Scientific Laboratory Report LA-DC-72-815, 1972.
20. Private Communication from R. E. Franz, Ballistic Research Laboratories, October 1971.
21. G. E. Hauver, "Shock-Induced Electrical Signals from Dielectrics," Fifth Symposium on Detonation, Pasadena, California, August 18-21, 1970, Office of Naval Research ACR-184, pp. 387-97.
22. G. E. Hauver, "Shock-Induced Polarization in Plastics. II. Experimental Study of Plexiglas and Polystyrene," J. Appl. Phys. Vol. 36, No. 7. July 1965, pp. 2113-8.
23. Private Communication from D. J. Edwards, Naval Ordnance Laboratory, 18 July 1973.
24. R. E. Franz, "Electrical Resistance Measurements on Shock Compressed Aluminum," Ballistic Research Laboratories Report No. 2073, November 1970. (AD #716328)

25. Private Communication from R. E. Franz, Ballistic Research Laboratories, November 1970.